Accepted Manuscript

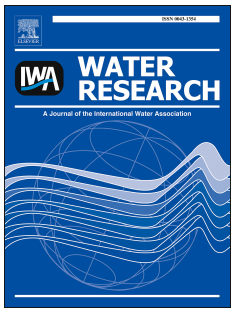

Fractionating various nutrient ions for resource recovery from swine wastewater using simultaneous anionic and cationic selective-electrodialysis

Zhi-Long Ye, Karel Ghyselbrecht, Annick Monballiu, Luc Pinoy, Boudewijn Meesschaert

PII: S0043-1354(19)30480-4

DOI: https://doi.org/10.1016/j.watres.2019.05.085

Reference: WR 14734

To appear in: *Water Research*

Received Date: 12 January 2019

Revised Date: 13 May 2019

Accepted Date: 25 May 2019

Please cite this article as: Ye, Z.-L., Ghyselbrecht, K., Monballiu, A., Pinoy, L., Meesschaert, B., Fractionating various nutrient ions for resource recovery from swine wastewater using simultaneous anionic and cationic selective-electrodialysis, *Water Research* (2019), doi: https://doi.org/10.1016/j.watres.2019.05.085.

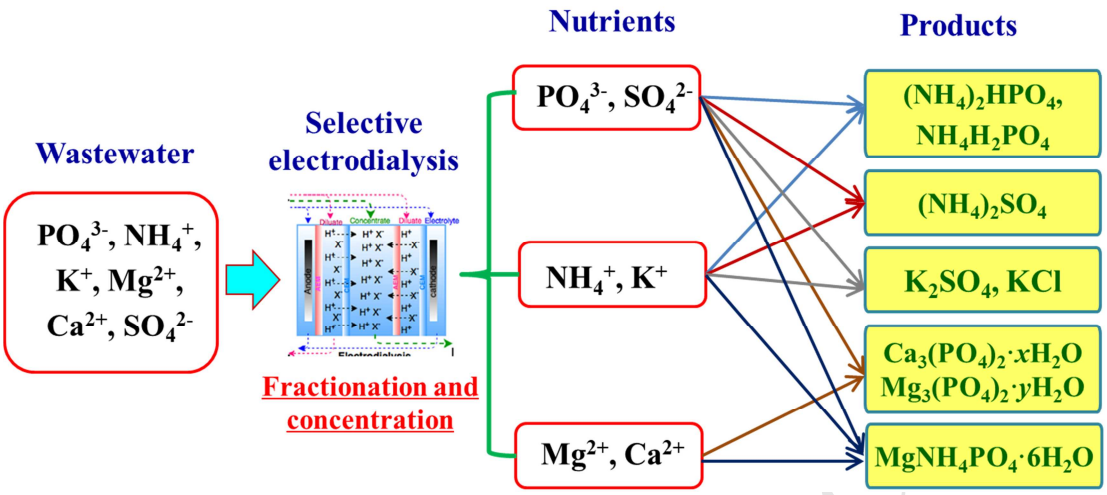

Fractionating various nutrient ions for resource recovery from swine wastewater using simultaneous anionic and cationic selective-electrodialysis

Zhi-Long Ye [a,b,*], Karel Ghyselbrecht [b], Annick Monballiu [b], Luc Pinoy [c], Boudewijn Meesschaert [b,*]

[a] Key Laboratory of Urban Pollutant Conversion, Institute of Urban Environment, Chinese Academy of Sciences, No. 1799 Jimei Road, Xiamen City, Fujian 361021, China.

[b] Cluster for Bio-engineering, Department of Microbial and Molecular Systems, Faculty of Engineering Technology, KU Leuven Campus Bruges, Spoorwegstraat 12, 8200 Brugge, Belgium.

[c] Cluster for Sustainable Chemical Process Technology, Department of Chemical Engineering, KU Leuven, Technology Campus Ghent, Gebroeders De Smetstraat 1, B-9000 Gent, Belgium.

*Corresponding author:

Zhi-Long Ye, E-mail address: zlye@iue.ac.cn

Boudewijn Meesschaert, E-mail address: boudewijn.meesschaert@kuleuven.be

Abstract

Different from current nutrient recovery technologies of recovering one or two nutrient components (PO_4^{3-} or NH_4^+) from wastewater, this study aimed to fractionate various nutrient anions and cations simultaneously, including PO_4^{3-}, SO_4^{2-}, NH_4^+, K^+, Mg^{2+} and Ca^{2+}, into several streams. The recovered streams could be further paired together to produce high-value products. A novel electrodialysis process was developed by integrating monovalent selective anion and cation exchange membranes into an electrodialysis stack. Results revealed that nutrient recovery was achieved effectively by fractionating PO_4^{3-} and SO_4^{2-} into the anionic product stream, whereas bivalent cations (Mg^{2+} and Ca^{2+}) were extracted in the cationic product stream and the monovalent cations (K^+ and NH_4^+) were concentrated in the brine stream. For the permeation capabilities of anions, SO_4^{2-} and Cl^- possessed the higher preference, whereas PO_4^{3-} permeated the membrane more difficult. As to the cations, the permeation sequence was: $NH_4^+ \approx K^+ > Ca^{2+} > Mg^{2+} \approx Na^+$. Enhancing voltage values not only promoted ion migration rates, but also led to the increase of energy consumption. Although elevating initial phosphate concentration in the anionic product streams from 60 mg/L to 470 mg/L did not influence phosphate fractionation significantly, the current efficiency decreased from 3.55% to 0.65% and a remarkable increased of energy consumption from 29.42 kWh/kg NaH_2PO_4 to 160.13 kWh/kg NaH_2PO_4 was observed. Further experiments were conducted for phosphorus recovery by pairing two recovered product streams, which revealed that phosphate precipitation could be achieved by using inherent Ca^{2+} and Mg^{2+} in the wastewater

without dosing external cation sources.

Keyword: Phosphorus recovery; Nutrient; Electrodialysis; Membrane; Wastewater

1. Introduction

Due to the quick economic growth and urbanization in the developing countries in past decades, a numerous demand on pork provision and pig farming has been triggered. For instance, pig production in China has risen from 412 million in Year 1996 to 685 million in Year 2016 (NBSPRC, 2017). Accordingly, a large amount of phosphorus and ammonium discharged from swine wastewater are accelerating environmental deterioration (Lin et al., 2014; Bai et al., 2014), which has raised concern worldwide. From another aspect, the quick urbanization resulted with the acceleration of the depletion of natural resources, which has increased pressures for providing sufficient fertilizer to the agriculture (Xie et al., 2016). It has been widely accepted that the macronutrients in the wastewater streams, such as PO_4-P, NH_4-N and K, could provide a substantial fraction of global requirement (Batstone et al., 2015; Mehta et al., 2016). Therefore, developing new processes for enhancing resource recovery from wastewater is necessary and critical.

Traditionally, since it contains abundant valuable resources of phosphorus, nitrogen and potassium, digestive swine wastewater is directly utilized as fertilizer and soil amendment for the agriculture (Nkoa, 2014). However, there are debates that the use of biogas stream on the land may pose risks of atmospheric and nutrient pollutions, soil contaminations (heavy metals, antibiotics, soil salinization etc.) in the

environment (Nkoa, 2014). Presently, there are several environment-friendly technologies developed to recover nutrient from waste streams, including chemical precipitation, adsorption, magnetic separation, algae and proteobacteria accumulation (Mehta et al., 2015). For the nutrient resources worldwide, phosphorus is a nonrenewable resource and is becoming progressively limited with supply uncertainty. In recent years, the consumption of phosphorus ores is accelerating (Mehta et al., 2015), and subsequently phosphate rock is listed as a critical raw material in many countries (Taddeo et al., 2016). Recovering phosphorus from waste streams has been regarded as an important mean of retarding the depletion of phosphorus reserves worldwide (Lee et al., 2018; Zhou et al., 2017).

Among the phosphorus recovery technologies, the precipitation of magnesium phosphate or calcium phosphate, such as struvite ($MgNH_4PO_4 \cdot 6H_2O$) and calcium phosphate ($Ca_3(PO_4)_2 \cdot xH_2O$), is predominantly used in wastewater with rich phosphorus and ammonium, such as digestive livestock wastewater and sludge slurry, urine (Abel-Denee et al., 2018; Kim et al., 2018; Desmidt et al., 2015). The recovered products can be used directly as fertilizers on the agriculture. However, the efficiency of phosphorus recovery is limited, since the phosphate concentration in the waste streams was required above 90 mg/L or pH higher than 9.0 (Xie et al., 2016; Zhang et al., 2013). Low phosphate concentration (20-50 mg/L) resulted in either low phosphate recovery or much more alkali addition to reach extreme high pH values, which made phosphorus recovery not a cost efficient process (Zhang et al., 2013; Xie et al., 2016). Besides, dosing divalent cation (Mg^{2+} or Ca^{2+}) chemicals to trigger

phosphate precipitation is another limiting factor for phosphorus recovery, since it contributes a major part of the total costs (Hövelmann et al., 2016). Several cheap cation agents, such as CaO, MgO, $Mg(OH)_2$, brucite and brine were investigated as the cost-effective sources (Li et al., 2018; Shen et al., 2016; Hövelmann et al., 2016; Liu et al., 2013). From another point of view, the digestive waste stream contains abundant Ca^{2+} and Mg^{2+} with the concentration range of 40-200 mg/L (Ye et al., 2011; Herrmann et al., 2016), which can be used as the potential sources for phosphate precipitation. Nevertheless, their existing concentrations are insufficient to reach proper supersaturation for phosphate precipitation. Therefore, exploring methods to enrich phosphate and divalent cations in the waste streams would be very beneficial, thereby significantly enhancing the potential and efficiency of phosphorus recovery from wastewater.

Electrodialysis is an electrochemical membrane process using the electrical field as driving force to separate and concentrate ionic components from the electrolytes. For the industrial application, electrodialysis is accepted with the advantages of environmental friendliness, convenient operation and cost-effectiveness, and has been used in many areas, including seawater desalination, wastewater and brackish water treatment (Reig et al., 2014; Zhang et al., 2017; Ye et al., 2018). Recently, electrodialysis equipped with selective cation or anion exchange membranes is developed and employed on the fractionation of valuable products, such as lithium and sodium formate (Ji et al., 2017; Selvaraj et al., 2018), and heavy metal removal (Gherasim et al., 2014). The application of selective electrodialysis with monovalent

exchange membranes on the recovery of one or two nutrient components (phosphate or ammonium) has already been investigated, and the fractionation was successfully performed (Zhang et al., 2013; Tran et al., 2015; Wang et al., 2015; Xie et al., 2016; Liu et al., 2017; Ward et al., 2018; Shi et al., 2018).

Different from the previous researches, the present study focused on various nutrient ions in the wastewater, i.e. PO_4^{3-}, SO_4^{2-}, NH_4^+, K^+, Mg^{2+} and Ca^{2+}, and aimed to develop a novel electrodialysis method to fractionate these ions into different streams. This was critical, as the recovered streams could be paired together to produce possible down-stream products (Figure 1), such as $NH_4H_2PO_4$, $(NH_4)_2SO_4$, $Ca_3(PO_4)_2 \cdot xH_2O$, $Mg_3(PO_4)_2 \cdot yH_2O$ and $MgNH_4PO_4 \cdot 6H_2O$. From another aspect, this method could not only concentrate nutrient ions, but also overcome the shortage of phosphorus recovery by providing a choice of using inherent Ca^{2+} and Mg^{2+} in the wastewater as the cation sources for phosphate precipitation. Accordingly, a novel electrodialysis process was developed by integrating monovalent selective anion exchange membranes and monovalent selective cation exchange membranes into a conventional electrodialysis stack, and was employed for the desalination and nutrient recovery from digestive swine wastewater. The operational parameters, including voltage, current density and initial phosphate concentration, were examined. Furthermore, two different product streams, one containing anions of PO_4^{3-} and SO_4^{2-}, the other with cations of Mg^{2+} and Ca^{2+}, were paired for phosphate precipitation without dosing other chemicals. Also, the permeation capabilities of various ions under different operational conditions and the recovery performance were evaluated.

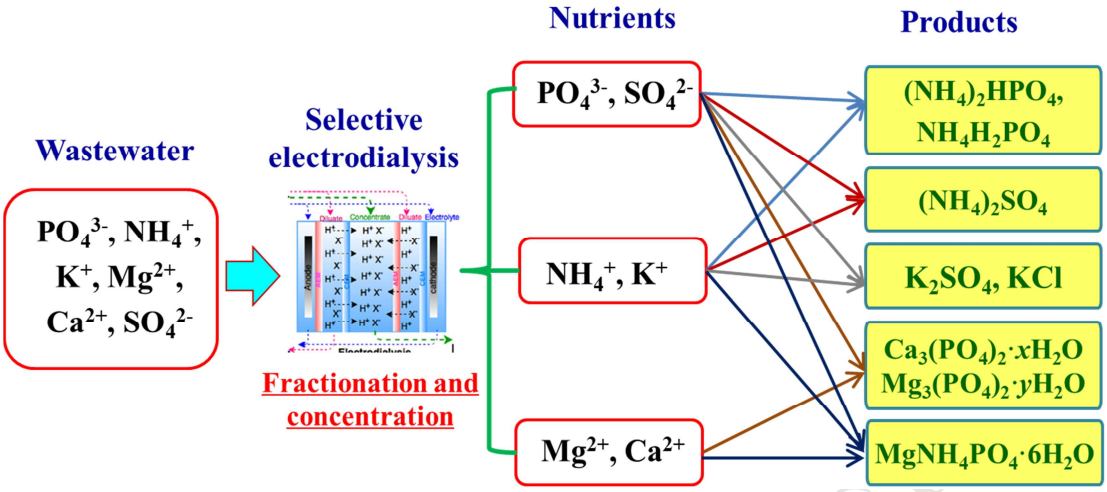

Figure 1 Possible down-stream products generated by pairing different nutrient streams together.

2. Materials and methods

2.1. Materials

Chemical compositions and their concentration levels of the simulated swine wastewater (feed stream) were referred according to the description of Shen et al. (2016) and Ye et al. (2018). The feed stream and the initial compositions of other streams were presented in Table 1. The chemicals used were of analytical grade, and deionized water was used throughout the experiments.

Five types of membranes used in the experiments were obtained from PCA GmbH, Germany, including standard cation exchange membrane (PC-SK), standard anion exchange membrane (PC-SA), monovalent selective anion exchange membrane (PC-MVA), monovalent selective cation exchange membrane (PC-MVK) and end cation-exchange membrane (PC-SC). All the membranes have active areas of 8 cm × 8 cm. The properties of the membranes are presented in Table 2.

Table 1

Table 2

2.2. Experimental setup

2.2.1. Electrodialysis stack

The assembled electrodialysis stack was constructed by two electrodes made of titanium wire (PCA GmbH Ltd., Germany) with the diameter at 2.5 mm coated with ruthenium oxide, PC-SA membranes, PC-SK membranes, PC-MVK membranes, PC-MVA membranes and electrodialysis spacers, as shown in Figure 2. The configuration of the electrodialysis stack contained five repeating units consisting of 5 PC-MVK membranes, 5 PC-MVA membranes, 5 PC-SA membranes, 4 PC-SK membranes and 2 PC-SC end membranes. From the anode to the cathode, a PC-SK membrane, a PC-MVK membrane, a PC-MVA membrane and a PC-SA membrane were installed in order. A spacer with a thickness of 0.5 mm was inserted in between every two membranes. A power supply (DELTA ELEKTRONIKA ES 030-10, Netherlands) was used to provide stable voltage or current for the electrodialysis experiments.

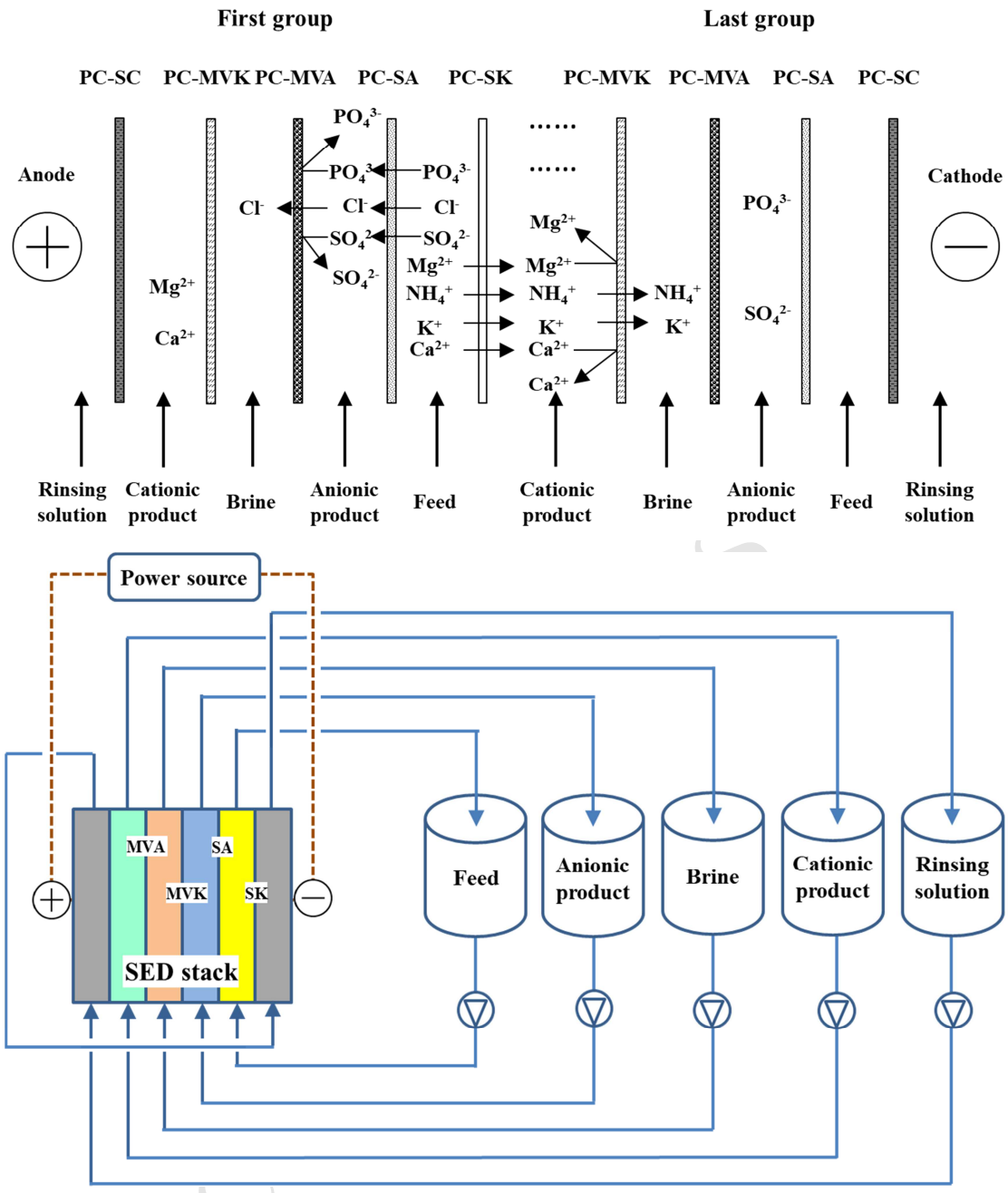

Figure 2 Configuration of the electrodialysis stack installed with different types of membranes (A) and schematic diagram of the selective electrodialysis setup (B).

The electrodialysis configuration consisted of five closed loops, including the anionic product, cationic product, brine, feed and electrode rinsing streams. These streams initially contained certain types of electrolyte solutions, as presented in Table 1. For each stream, it was connected to an external reservoir, so as to maintain

continuous recirculation. In each experimental run, the initial volume of feed solution was 2.0 L and the volumetric ratio of feed, anionic product, cationic product and brine streams was kept at 2:1:1:1. During the experiments, the flow velocity of each stream was set at 10.62 cm/s by using an impeller pump with the pipe diameter at 1 cm. In order to eliminate the air bubbles in the stack (Eisaman et al., 2011), each stream was circulated for 1 min before starting the experiments.

2.2.2. Experimental procedure

Before the experiments, the determination of limiting current density was conducted for the optimal electrodialysis operation and avoiding redox reactions. The determination method of limiting current density was described by previous studies (Ghyselbrecht et al., 2013; Ward et al., 2018). The performance of nutrient fractionation is determined by the electrodialysis configuration, the properties of wastewater as well as the operation conditions, such as voltage, ion concentrations etc. In the present study, the operational modes (constant voltage and constant current density), effects of voltage and phosphate concentration were examined.

For the electrodialysis operation, there are two common operation power modes, i.e. constant current and constant voltage. In case constant current is applied, the continuous operation will be implemented. In case constant voltage is applied, the batch operation will be conducted. In the present study, constant voltage and constant current were investigated respectively in the experiments to find which one is preferable for nutrient recovery from the wastewater. 7.8 V for the constant voltage and 45.3 A/m^2 for the constant current were respectively selected as operational

196 parameter, which were based on the preliminary experiments by comparing the
197 profiles of conductivity changes in the feed, brine and product streams. After that,
198 constant voltage was selected for the following experiments, and its effects on
199 selective electrodialysis were investigated by setting the voltage at 6, 7, 8, 9 and 10 V,
200 respectively.

201 Among the nutrient compositions in the wastewater, phosphorus is more
202 important due to the depletion of phosphorus resources worldwide (Hukari et al., 2016;
203 Agrawal et al., 2018). Hence, phosphate concentration was selected as the examined
204 parameter in the current study. The experiments were carried out by setting initial
205 PO_4-P in the anionic product stream at 60, 180, 270 and 470 mg/L, respectively,
206 which could reveal the capacity of anionic product stream of extracting phosphate.

207 After the electrodialysis experiments, the fractionating streams contained
208 different nutrient ions, i.e. the brine stream with NH_4^+ and K^+ ions, the anionic
209 product stream with PO_4^{3-} and SO_4^{2-} ions and the cationic product stream with Mg^{2+}
210 and Ca^{2+} ions, respectively. These streams could be further processed as nutrient
211 products, or could be paired together to produce the down-stream products, such as
212 $NH_4H_2PO_4$, $(NH_4)_2SO_4$, $Ca_3(PO_4)_2 \cdot xH_2O$ and $MgNH_4PO_4 \cdot 6H_2O$ (Figure 1). In the
213 present study, the anionic and cationic product streams obtained from the previous
214 experimental runs at constant voltage of 6, 8 and 10 V were mixed in proportion for
215 phosphate recovery. Desired volumes of the anionic and cationic product streams
216 were calculated and mixed to maintain Mg:P molar ratio at 1.2:1, and pH value was
217 kept at 10.0 by dosing 2 mol/L NaOH to perform phosphate precipitation. After 60

min stirring, the liquor was settled for 120 min, and the precipitates were collected by 5000 rpm centrifugation.

2.3. Analytical methods

An ion chromatography (883 Basic IC Plus, Metrohm, Switzerland) was employed for ion analyses. For anions (PO_4^{3-}, SO_4^{2-} and Cl^-), an anion column of Metrosep A Supp 5-150/4.0 was applied with 3.2 mM Na_2CO_3 and 1.0 mM $NaHCO_3$ as eluent at a constant flow rate of 0.7 mL/min, whereas a cation column of Metrosep C4-150/4.0 (Methrohm, Switzerland) was adopted for cation determination (Na^+, K^+, NH_4^+, Mg^{2+} and Ca^{2+}) with 0.7 mM dipicolinic acid and 1.7 mM HNO_3 as eluent at a constant flow rate of 0.9 mL/min. Conductivity and pH were measured by LF318 conductivity meter (WTW, Germany) and pH/Ion S220FE pH meter (Mettler-Toledo, Germany), respectively.

2.4. Data analyses

The energy consumption (*E*) is a parameter for economic evaluation and was determined by the following equation, which has been described by Zhang et al. (2017).

$$E = \frac{\int_0^t U.I.dt}{(C_t.V_t - C_0.V_0).\frac{M_b}{M_a}}$$

where C_0 and Ct are the initial concentration and the concentration at time t of fractionating ions in the product compartment, U the voltage the for interval time (Δt), V_0 and V_t the circulated volume of the product stream at time 0 resp. time t, M_a *and* M_b the molecular weight of cation (or anion) and its chloride (or sodium salt).

The current efficiency of ion A (η_A) is defined as the ratio of the electrical charge

239 used for the transport of ion A to the total electrical current charge (Ghyselbrecht et al.,
240 2013), with the equation as follows:

$$\eta_A = \frac{\left(\frac{\Delta m_A(t)}{M_A}\right) zF}{\int_0^t nIdt} \times 100(\%) = \frac{(C_t \times V_t - C_0 \times V_0) zF/M_A}{\int_0^t nIdt} \times 100\%$$

241 where *z* is the charge of ion A, *F* the Faraday constant (96,500 C/mol), $\Delta m_A(t)$ the
242 weight of transformed ion A at time *t* into the product stream, *n* the number of
243 repeating units (*n*=5), *t* the time periods, *I* the current during interval time (Δt), M_A
244 the molar mass of ion A, C_t the ion concentration, V_t the volume of the anionic or
245 cationic product stream.

246 The ionic migration rate (M_r) for each ion was determined as described by Chen
247 et al. (2018), where the ion transports in a certain period:

$$M_r \ (\text{mmol}/m^2 \cdot \text{min}) = \frac{\Delta C_{ct} \times V_{ct}}{S \times t}$$

248 where C_{ct} is electrolytic concentration (mol/L) in the product or brine streams
249 dependent on the fractionating ions, V_{ct} the total volume of the product or brine
250 streams (L), S the effective area of membrane stack (m^2).

251 The recovery efficiency of nutrient ions was defined as the ratio of the amount of
252 nutrient ions in the product streams or NH_4^+ and K^+ in the brine compartment to the
253 initial nutrient ions in the feed stream. Hence, the calculation of fractionation ratio (*R*)
254 for nutrient ions from the wastewater to the product stream was based on the
255 following equation:

$$R = \frac{C_{P,B}(t)V_{P,B}(t) - C_{P,B}(0)V_{P,B}(0)}{C_F(0)V_F(0) - C_F(t)V_F(t)} \times 100\%$$

256 where $C_{P,B}(t)$ and $C_F(t)$ are the concentrations of nutrient ions at time *t* in the product

257 streams (PO_4^{3-} and SO_4^{2-}, Mg^{2+} and Ca^{2+}) or the brine stream (NH_4^+ and K^+), and the
258 feed stream, coupling with their volume $V_{P,B}(t)$ and $V_F(t)$, respectively. NH_4^+ and K^+
259 moved longer distances, i.e. from the feed compartment, passing through the cationic
260 product compartment, and finally going into the brine chamber. Therefore, it was
261 expected that the maximum R value of NH_4^+ and K^+ during the experiments would be
262 lower than other ions. In case the electrodialysis operates with the continuous mode in
263 the future pilot-scale experiments, the values of R on NH_4^+ and K^+ will significantly
264 enhance.

265 **3. Results and discussion**

266 **3.1. Operational mode**

267 There are two common operation power modes for the electrodialysis, including
268 constant current and constant voltage. As for the swine wastewater, it normally
269 contains various ions with a relatively low electrical conductivity (8-12 mS/cm),
270 which might display different ion transport behavior under different operational
271 modes. The profiles of conductivity and pH under different operational modes were
272 investigated. As shown in Figure S1, the decrease rate of conductivity in the feed
273 streams was 0.057 mS/(cm·min) for constant current, while 0.059 mS/(cm·min) was
274 observed for constant voltage. Besides, there different operation modes shared similar
275 pH variation as displayed in Figure S2. The conductivity variation in the anionic and
276 cationic product streams displayed similar profiles, which also indicated that the
277 desalination performance in both modes was not significantly different.

278

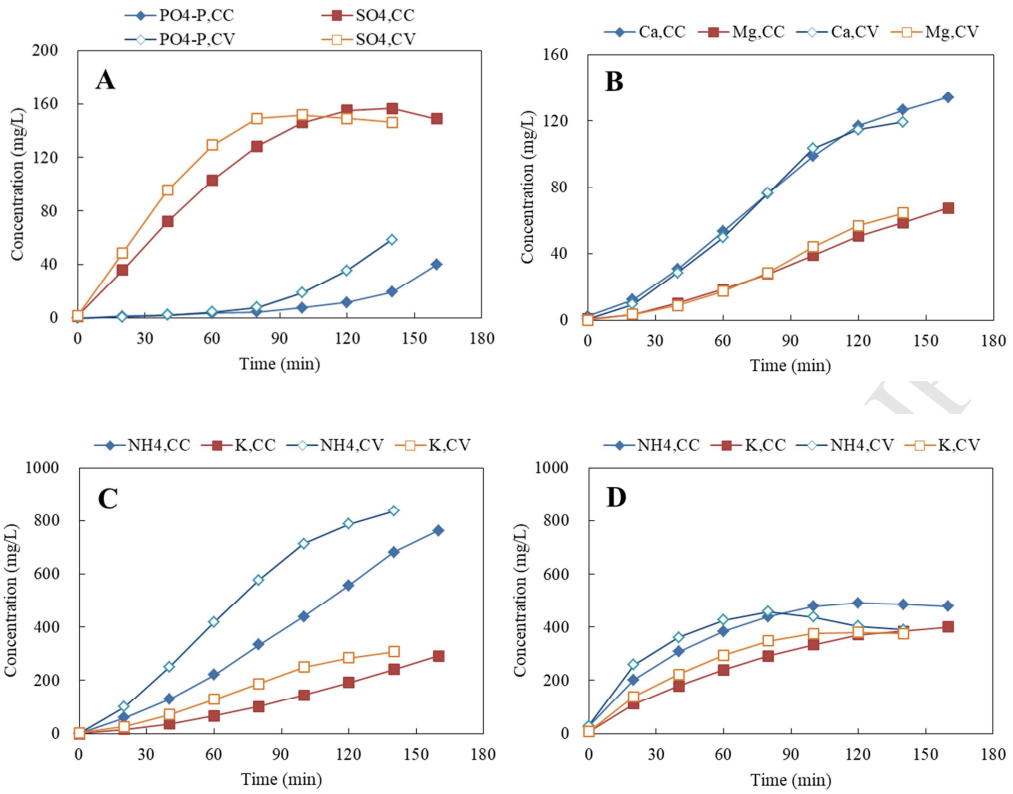

Figure 3 Concentrations of PO_4^{3-}-P and SO_4^{2-} in the anionic product (A), Mg^{2+} and Ca^{2+} in the cationic product (B), K^+ and NH_4^+ in the brine stream (C) and the cationic product (D) under different operation modes. CV, constant voltage, CC, constant current.

According to the configuration of electrodialysis stack (Figure 2), nutrient anions (PO_4^{3-} and SO_4^{2-}) were fractionated in the anionic product stream, whereas bivalent nutrient cations (Mg^{2+} and Ca^{2+}) were extracted in the cationic product stream and monovalent cations (K^+ and NH_4^+) were concentrated in the brine stream. The profiles of various ions in relevant streams were displayed in Figure 3. After the electrodialysis operation, the mode of constant voltage recovered 58.4 mg/L PO_4^{3-}-P, 146.0 mg/L SO_4^{2-}, 64.4 mg/L Mg^{2+}, 119.2 mg/L Ca^{2+}, 307.0 mg/L K^+ and 837.6 mg/L NH_4^+-N, similar to 39.9 mg/L PO_4^{3-}-P, 148.8 mg/L SO_4^{2-}, 67.5 mg/L Mg^{2+}, 134.1

293 mg/L Ca^{2+}, 291.1 mg/L K^{+} and 763.2 mg/L NH_4^{+} under constant current. This
294 observation indicated that both electrodialysis operation modes could achieve similar
295 performance on simultaneous nutrient ion fractionation, which was also confirmed by
296 the comparisons of fractionation, energy consumption and current efficiency ratio as
297 presented in Table 3. It should be noted that compared to previous researches, nutrient
298 recovery in this selective electrodialysis system displayed different efficiencies on
299 energy consumption. Take the operation mode of constant voltage for instances, this
300 selective electrodialysis was favor to fractionate NH_4^{+} and SO_4^{2-} with lower energy
301 consumption at 0.783 kWh/kg NH_4-N and 6.638 kWh/kg Ca, compared to 4.9
302 kWh/kg NH_4-N and 7.544 kWh/kg Ca reported in literature (Li et al., 2016; Ye et al.,
303 2018). The energy consumptions on magnesium and sulfate were 6.103 kWh/kg Mg
304 and 17.995 kWh/kg SO_4, respectively, much higher than those reported in previous
305 researches (Ye et al., 2018; Li et al., 2016). As to phosphate, 28.38 kWh/kg PO_4
306 energy was consumed to recover phosphate, not much higher to 29.3 kWh/kg PO_4 as
307 reported by other researchers (Xie et al., 2016). However, the profiles of voltage and
308 current variation (Figure 4) indicated that constant voltage was more preferable than
309 constant current for the fractionation of nutrient ions from swine wastewater. For
310 constant voltage, a steady decrease of current was observed, whereas a drastic
311 increase of voltage to reach 15.7 V at the ending stage was detected in the mode of
312 constant current. This was because under constant current, more and more ions
313 transported from the feed stream into the product and brine chambers and
314 consequently the electrical resistance of the feed stream increased greatly. Such high

voltage exceeded the membrane affordability and would damage the membrane in a long operation.

Table 3

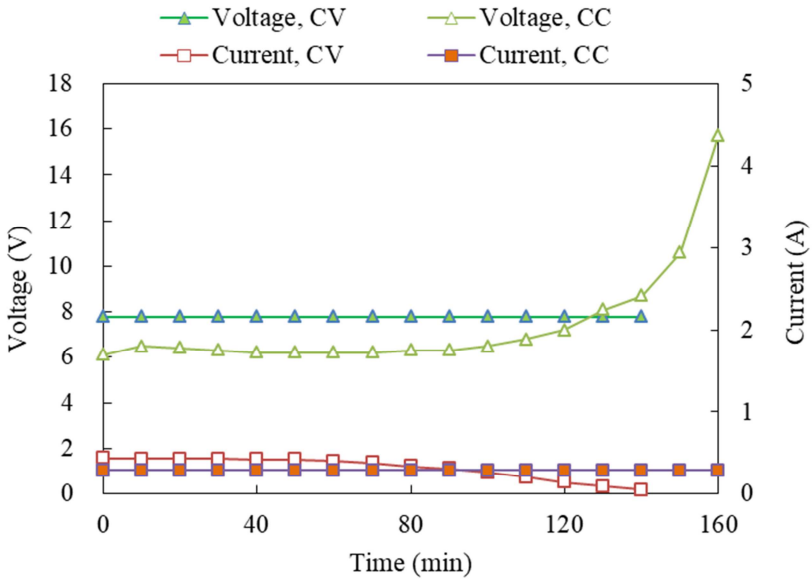

Figure 4 Changes of voltage and current under different operational modes. CV, constant voltage; CC, constant current.

From Figure 3 and Table 3, it was observed that different ions possessed different permeation capabilities. The dimensionless masses of ions (mass at any time divided by the initial mass) in the feed compartment was employed to elaborate the permeation preference of different anions (PO_4^{3-}, SO_4^{2-} and Cl^-) and cations (Mg^{2+}, Ca^{2+}, K^+, NH_4^+ and Na^+). The lower position the curves located, the faster permeation the ions achieved. Take the mode under constant voltage for instance, for anions, SO_4^{2-} and Cl^- possessed the higher permeating preference, whereas PO_4^{3-} permeated the membrane more difficult (Figure 5A). For cations, the permeation sequence for

the process was: $NH_4^+ \approx K^+ > Ca^{2+} > Mg^{2+} \approx Na^+$. It has been reported that hydrated radius size played vital roles in the effects of coexisting ions in the electrodialysis process (Rotties et al., 2015; Chen et al., 2018; Shi et al., 2018). The hydrated radius of anions and cations were collected from the literature and listed in Table 4. It could be seen that the permeation performances of most ions (except Cl^- and Na^+) were compliant to their hydrated radius sequence. Nevertheless, Cl^- and Na^+ possessed slower permeating behaviors uncorresponding to their smaller hydrated radius sizes (Cl^-, 0.225 nm; Na^+, 0.358 nm), as shown in Figure 5. Considering that the anionic and cationic product compartments contained high NaCl (0.1 mol/L) contents as the electrolyte, the effects of steric hindrance led to the reduction of Cl^- and Na^+ mobilities. Similar results were reported by Nie et al., (2017) and Chen et al., (2018).

Table 4

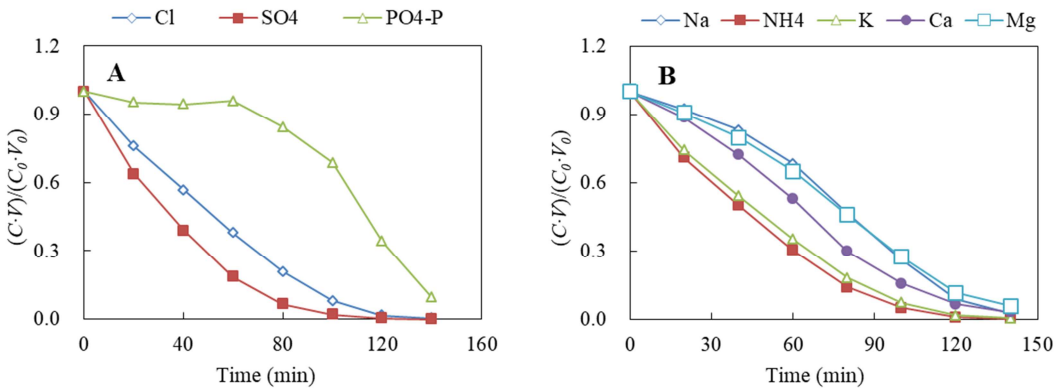

Figure 5 Dimensionless mass of various anions and cations under constant voltage.

3.2. Influence of voltage

The investigation of voltage from 6V to 10V on nutrient ion extraction was

conducted. Figure S3 showed the effects of voltage on the current and conductivity variations in the feed stream. Larger voltage improved more ion transport with higher initial current observed. As the process continued, more ions migrated from the feed compartment to the product and brine compartments with the electrical resistance of the stack ascending rapidly, and consequently the current declined significantly (Figure S3A). Higher voltages forced the ions to pass through the membranes faster, which resulted in the quicker desalination rates (Figure S3B).

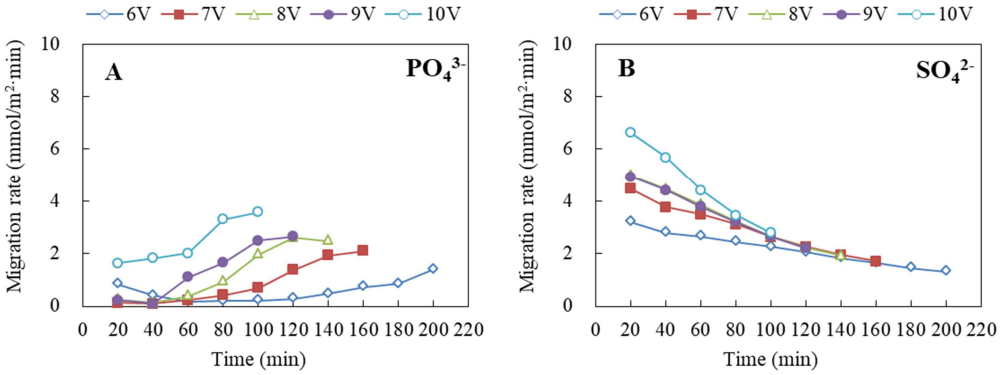

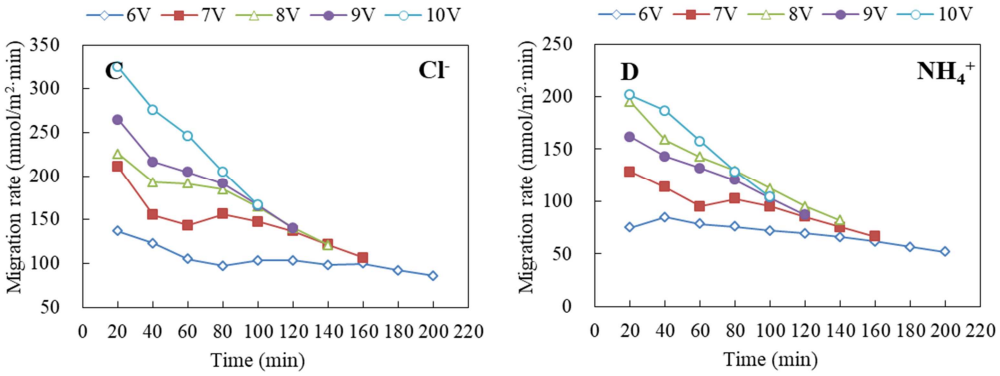

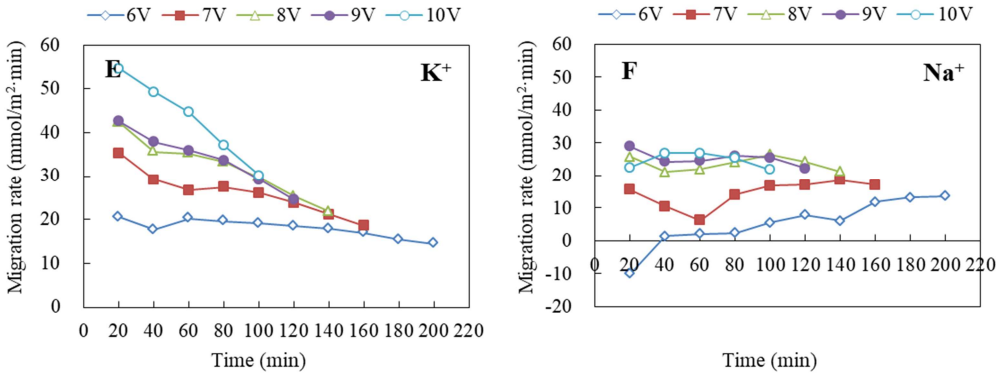

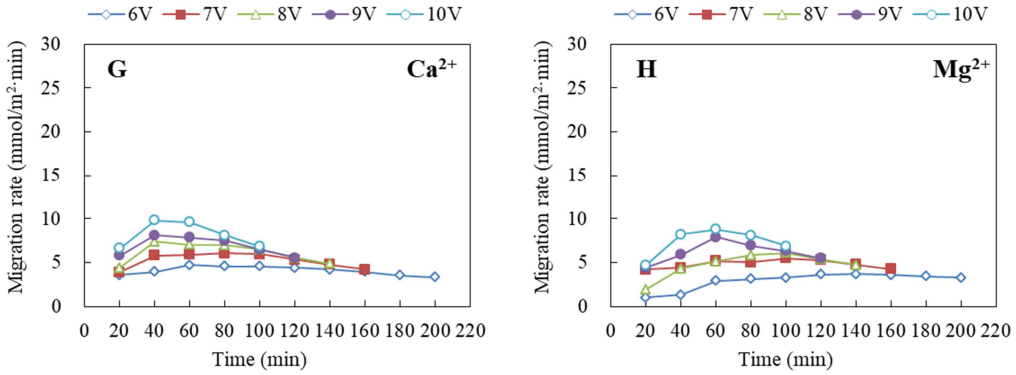

Figure 6 Ionic migration rates of PO_4^{3-} (A), SO_4^{2-} (B), Cl^- (C), NH_4^+ (D), K^+ (E), Na^+ (F), Ca^{2+} (G) and Mg^{2+} (H) during the electrodialysis process.

Under such voltage enhancement, the changes of various anions and cations were presented in Figure S4, which suggested that increasing voltage would speed up the ions permeation. The ionic migration rate (M_r) for each ion in the electrodialysis process was determined and displayed in Figure 6. It could be seen that all monovalent ions, including Cl^-, NH_4^+, K^+ and Na^+, showed significant downward trends with the increase of operation time, and they possessed the higher migration rates than divalent and trivalent ions. As for the divalent ions, including SO_4^{2-} (Figure 6B), Ca^{2+} (Figure 6G) and Mg^{2+} (Figure 6H), they had lower migration rates, according to their variations in the Y-axis. Enhancing voltage values speeded up the decline of SO_4^{2-} migration rates, whereas the profiles of slight increase following with gradual decline were observed for Ca^{2+} (Figure 6G) and Mg^{2+} (Figure 6H) ions. As to the trivalent ion, PO_4^{3-}, it showed a significantly different shape of transportation rate with continuous increase (Figure 6A).

It was clear that the voltage increment from 6 V to 10 V not only promoted ion migration rates, but also lead to the increase of energy consumption (Table 5). This

377 was because increasing voltage augmented the electric field and resultant driving
378 force for ion transport through the electrodialysis compartments (Masigol et al., 2012).
379 From another aspect, on the basis of Table 5 and the market information (MOLBASE
380 E-commerce platform, www.molbase.com) where the prices of the indivisually
381 recovered salts were $MgCl_2$ 3.16 €/kg, $CaCl_2$ 0.79 €/kg, NaH_2PO_4 3.72 €/kg, Na_2SO_4
382 3.18 €/kg, NH_4Cl 6.76 €/kg and KCl 2.89 €/kg, the benefits of energy consumption
383 would be $MgCl_2$ 0.13-0.18 €/kWh, $CaCl_2$ 0.04-0.05 €/kWh, NaH_2PO_4 0.11-0.19
384 €/kWh, Na_2SO_4 0.09-0.10 €/kWh, NH_4Cl 1.53-3.89 €/kWh and KCl 0.16-0.43 €/kWh,
385 respectively. Nevertheless, according to the variation of current efficiency (Table 5),
386 the application of higher voltages did not mean that the electrical power could be
387 effectively utilized for every ion migration. Different ions displayed different
388 migration performances. It should be pointed out that the ion permeation capabilities
389 were not only determined by the effects of electric double layer and steric hindrance
390 on the cation-exchange membrane (Nie et al., 2017), but also influenced by the
391 operation conditions, including voltage, current density and ion concentrations (Reig
392 et al., 2014; Li et al., 2016). As for the monovalent ions, enhancing voltage
393 accelerated their migration (Figure 6C, D and E) due to their small hydrated radius
394 size (Rotties et al., 2015; Chen et al., 2018; Shi et al., 2018). The unusual movement
395 of Na^+ ion in the experiments was ascribed to the effects of steric hindrance (Nie et al.,
396 2017), since the anionic and cationic product compartments contained high Na^+
397 concentration as the electrolyte.

398 ----------

399 Table 5

400 ----------

401 For the divalent anion, SO_4^{2-} had similar descending profiles of migration speed
402 (Figure 6B) to the monovalent ions, which could be ascribed to its medium size of
403 hydrated radius (Table 4), compared to those of Cl^- and PO_4^{3-}. As to the divalent
404 cations, i.e. Ca^{2+} (Figure 6G) and Mg^{2+} (Figure 6H), the profiles of their migration
405 rates displayed ascending trends in the early stage and declined gradually to the end of
406 experiments. Such variation indicated that there might have several functions existed
407 which impacted the transport of these cation ions. It has been reported that the
408 mobility of various cations was determined by their charges and the hydrated radius of
409 those coexisting cations (Chen et al., 2018; Nie et al., 2017). For Ca^{2+} and Mg^{2+}, they
410 possessed higher charge and higher hydrated radius (Table 4), and got the resultant of
411 lower mobility (Figure 6G and 6H) through the cation exchange membrane compared
412 to the monovalent cations (Na^+, K^+ and NH_4^+), which was consistent with the
413 previous researches (Tadimeti and Chattopadhyay, 2016; Nie et al., 2017). Besides,
414 Mg^{2+} and Ca^{2+} ions were preferentially adsorbed and accumulated on the interface of
415 cation exchange membrane, and thus enhanced the steric hindrance of divalent
416 transport (Nie et al., 2017; Chen et al., 2018). Under large values of applied voltage,
417 the effects of steric hindrance were amplified and led to the concentration polarization,
418 which in turn reduced the divalent cation migration (Ye et al., 2018). This was why
419 these divalent cations presented ascending trends in the early stage of electrodialysis
420 under higher voltages (Figure 6G and 6H).

Phosphate, as the trivalent ion, displayed different trend shapes on the migration rate in the electrodialysis process (Figure 6A). Previous research revealed that phosphate was transported slower when sulfate and chloride were present (Tran et al., 2015). This was because these co-existent anions competed with phosphate to be transported, and they moved across the membrane faster than phosphate due to their smaller hydrated size (Table 4). Besides, the higher driving force due to higher valence played a role in favorable transport of chloride and sulfate over phosphate (Geluwe et al., 2011), which explained that the migration rate of phosphate increased continuously in the experiments. Similar phenomena were reported in other studies (Tran et al., 2015; Shi et al., 2018).

3.3. Influence of phosphate concentration in the product stream

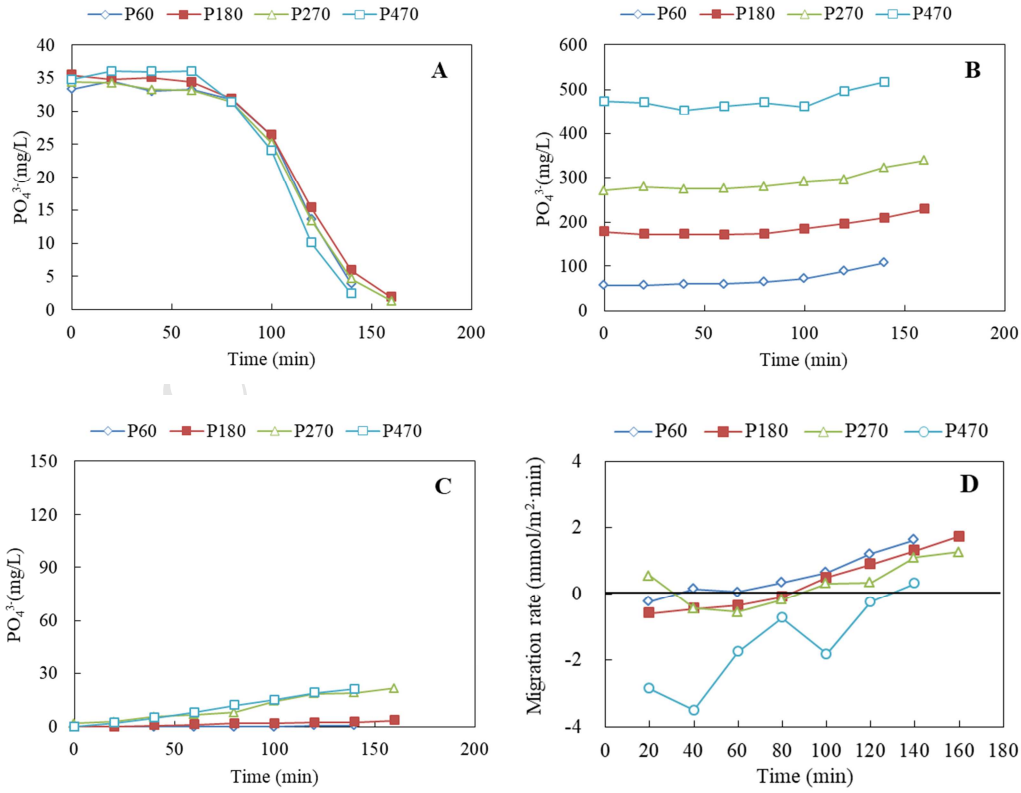

Figure 7 Variation of PO_4^{3-}-P concentrations in the feed stream (A), anionic product

435 stream (B) and brine stream (C), and the migration rate of PO_4^{3-}-P in the anionic
436 product stream (D) under different initial phosphate concentration. P60, P180, P270
437 and P470 represent the initial phosphorus concentrations in the anionic product stream
438 at 60, 180, 270 and 470 mg/L, respectively.

439 The effects of initial nutrient ion concentration in the product streams are of great
440 importance to evaluate the optimum domain of applicability of the selective
441 electrodialysis process investigated. In the present study, the initial phosphate
442 concentration in the anionic product stream was selected as the examined parameter.
443 As shown in Figure 7A and 7B, elevating PO_4^{3-}-P concentration from 60 mg/L to 470
444 mg/L in the anionic product stream insignificantly altered the profiles of phosphate
445 concentrations in the feed and anionic product streams. Nevertheless, under high
446 initial phosphate concentrations, a certain amount of phosphate (approximately 21
447 mg/L) permeating into the brine chamber was detected (Figure 7C), which did not
448 occurr in previous experiments. Besides, the rate of phosphate migrating into the
449 anionic product chamber was calculated, and enhancing initial PO_4^{3-}-P concentrations
450 resulting in smaller migration rates were observed (Figure 7D). Further investigation
451 on energy consumption, current efficiency and extraction ratio (Table 6) revealed that
452 increasing initial phosphate concentrations in the anionic product stream led to the
453 obvious declines of current efficiency and phosphorus extraction ratio, and gave rise
454 to a remarkable enhancement of energy efficiency as well.

455 ----------

456 Table 6

457 ----------

458 For the continuous operation of electrodialysis, more and more nutrient ions
459 transport and accumulate in the product chambers, which may subsequently increase
460 the resistance of ion migration into the product streams and negatively impact the
461 performance of nutrient recovery. As shown in Figure 7 and Table 6, although
462 elevating phosphate concentrations in the anionic product stream insignificantly
463 impacted the extraction of phosphate from the feed compartment to the anionic
464 product compartment, a distinct hindrance was discovered based on the decrease of
465 migration rate (Figure 7D) and the augment of energy efficiency (Table 6). This was
466 because the existence of high phosphate concentrations in the anionic product
467 chamber augmented the steric hindrance and suppressed phosphate migration from the
468 neighboring feed chamber to the anionic product chamber, which was also confirmed
469 by the previous study (Geng et al., 2018). In addition, in case phosphate concentration
470 was enhanced to 270 mg/L in the anionic product chamber, a permeation of phosphate
471 into the brine chamber was detected (Figure 7C). For the ion movement in the
472 electrodialysis process, the driving forces included electrical field, molecular diffusion
473 and convection (Tado et al., 2016). The phenomenon of phosphate permeating into the
474 neighboring brine chamber was ascribed to molecular diffusion due to the osmotic
475 pressure of phosphate, generated from the anionic product stream (Tado et al., 2016).
476 Similar results were reported by other researches (Tedesco et al., 2016; Benneker et
477 al., 2018; Jia et al., 2018).

3.4. Phosphate recovery

After the electrodialysis process, the anionic product stream containing PO_4^{3-} and SO_4^{2-} ions and the cationic product stream with Mg^{2+} and Ca^{2+} cations were respectively withdrawn from the experiments which were operated under different voltages, and they were mixed for phosphate precipitation without dosing external cation sources. Table 7 presented the mmol/g and the molar ratios of the composition in the precipitates. The recovered solids contained calcium phosphate ($Ca_3(PO_4)_2 \cdot xH_2O$) and magnesium phosphate ($Mg_3(PO_4)_2 \cdot yH_2O$).

It has been known that for phosphate recovery from wastewater, the costs of magnesium or calcium sources are one of the key limiting factors for operation (Moerman et al., 2013; Hug and Udert, 2013; Wang et al., 2018). Although cheap cation agents, such as MgO, CaO, bittern and seawater (Ye et al., 2011; Lahav et al., 2013; Wang et al., 2018), were adopted for phosphate precipitation, the operation cost was not reduced significantly (Barbosa et al., 2016; Wang et al., 2018). This study provided another choice by using the inherent Ca^{2+} and Mg^{2+} in the wastewater as the cations sources for phosphate precipitation. As shown in Table 7, the fractionated Ca^{2+} and Mg^{2+} performed phosphate recovery from the wastewater. From another aspect, this outcome was conclusive that the separated streams originated from the selective electrodialysis process containing with various nutrient ions could be paired together to produce the valuable products, which was beneficial to nutrient recovery from wastewater.

Table 7

---

4. Conclusion

This research focused on the recovery of various nutrient ions in the wastewater, i.e. PO_4^{3-}, SO_4^{2-}, NH_4^+, K^+, Mg^{2+} and Ca^{2+}, and developed a novel electrodialysis process, which could fractionate nutrient anions and cations simultaneously from the wastewater. A designed electrodialysis system integrating standard cation and anion exchange membranes, and monovalent selective anion and cation exchange membranes was employed. Results showed that nutrient anions (PO_4^{3-} and SO_4^{2-}) were successfully fractionated in the anionic product stream, whereas bivalent nutrient cations (Mg^{2+} and Ca^{2+}) were extracted in the cationic product stream and monovalent cations (K^+ and NH_4^+) were concentrated in the brine stream. For the permeation capabilities of anions, SO_4^{2-} and Cl^- possessed the higher preference, whereas PO_4^{3-} permeated the membrane more difficult. As to the cations, the permeation sequence for the process was: $NH_4^+ \approx K^+ > Ca^{2+} > Mg^{2+} \approx Na^+$. Enhancing voltage values not only promoted ion migration rates, but also led to the increase of energy consumption. Increasing initial phosphate concentration in the anionic product streams insignificantly altered the profiles of phosphate concentrations in the feed and anionic product streams, but led to the declines of current efficiency and remarkable increases of energy consumption. Further experiments were conducted by mixing the anionic and cationic product streams, and phosphate recovery was achieved without dosing external Ca^{2+} and Mg^{2+} as the cation sources.

Acknowledgement

This work was supported by the China Scholarship Council (No. 201604910345), the TETRA-project HBC.2017.0029 of the Agency for Promotion of Innovation and Entrepreneurship of the Flemish Government in Belgium, and the China-Japanese Research Cooperative Program (No. 2016YFE0118000).

References

Abel-Denee, M., Abbott, T., Eskicioglu, C., 2018. Using mass struvite precipitation to remove recalcitrant nutrients and micropollutants from anaerobic digestion dewatering centrate. Water Res. 132, 292-300.

Agrawal, S., Guest, J.S., Cusick, R.D., 2018. Elucidating the impacts of initial supersaturation and seed crystal loading on struvite precipitation kinetics, fines production, and crystal growth. Water Res. 132, 252-259.

Bai, Z., Ma, L., Qin, W., Chen, Q., Oenema, O., Zhang, F., Changes in pig production in China and their effects on nitrogen and phosphorus use and losses. Environ. Sci. Technol. 48, 12742-9.

Barbosa, S.G., Peixoto, L., Meulman, B., Alves, M.M., Pereira, M.A., 2016. A design of experiments to assess phosphorous removal and crystal properties in struvite precipitation of source separated urine using different Mg sources. Chem. Eng. J. 298, 146-153.

Batstone, D.J., Hulsen, T., Mehta, C.M., Keller, J., 2015. Platforms for energy and

544 nutrient recovery from domestic wastewater: a review. Chemosphere 140, 2-11.
545 Benneker, A.M., Klomp, J., Lammertink, R.G.H., Wood, J.A., 2018. Influence of
546 temperature gradients on mono- and divalent ion transport in electrodialysis at
547 limiting currents. Desalination 443, 62-69.
548 Chen, Q., Ji, Z., Liu, J., Zhao, Y., Wang, S., Yuan, J., 2018. Development of
549 recovering lithium from brines by selective-electrodialysis: Effect of coexisting
550 cations on the migration of lithium. J. Membr. Sci. 548, 408-420
551 Desmidt, E., Ghyselbrecht, K., Zhang, Y., Pinoy, L., Van der Bruggen, B., Verstraete,
552 W., Rabaey, K., Meesschaert, B., 2015. Global phosphorus scarcity and full-Scale
553 P-recovery techniques: a review. Crit. Rev. Env. Sci. Technol. 45, 336–384.
554 Eisaman, M.D., Alvarado, L., Larner, D., Wang, P., Littau, K.A., 2011. CO_2
555 desorption using high-pressure bipolar membrane electrodialysis. Energy Environ.
556 Sci. 4, 4031-4037.
557 Geng, Y., Wang, Y., Pan, X., Sheng, G., 2018. Electricity generation and in situ
558 phosphate recovery from enhanced biological phosphorus removal sludge by
559 electrodialysis membrane bioreactor. Bioresour. Technol. 247, 471-476.
560 Gherasim, C.V., Krivcik, J., Mikulasek, P., 2014. Investigation of batch electrodialysis
561 process for removal of lead ions from aqueous solutions. Chem. Eng. J. 256,
562 324-334.
563 Ghyselbrecht, K., Huygebaert, M., Van der Bruggen, B., Ballet, R., Meesschaert, B.,
564 Pinoy, L., 2013. Desalination of an industrial saline water with conventional and
565 bipolar membrane electrodialysis. Desalination 318, 9-18.

566 Herrmann, D.D., Sampaio, S.C., Castaldelli, A.P.A., Tsutsumi, C.Y., Prior, M., 2016.
567 Association of swine wastewater and mineral fertilization on black oat production.
568 Engenharia Agrícola 36, 799-810.
569 Hövelmann, J., Putnis, C.V., 2016. In situ nanoscale imaging of struvite formation
570 during the dissolution of natural brucite: implications for phosphorus recovery
571 from wastewaters. Environ. Sci. Technol. 50, 13032-13041.
572 Hug, A., Udert, K.M., 2013. Struvite precipitation from urine with electrochemical
573 magnesium dosage. Water Res. 47 (1), 289 – 299.
574 Hukari, S., Hermann, L., Nättorp, A., 2016. From wastewater to fertilisers-Technical
575 overview and critical review of European legislation governing phosphorus
576 recycling. Sci. Total Environ. 542, 1127-1135.
577 Ji, Z., Chen, Q., Yuan, J., Liu, J., Zhao, Y., Feng, W., 2017. Preliminary study on
578 recovering lithium from high Mg^{2+}/Li^{+} ratio brines by electrodialysis. Sep. Purif.
579 Technol. 172, 168-177.
580 Jia, Y.X., Li, F.J., Chen, X., Wang, M., 2018. Model analysis on electrodialysis for
581 inorganic acid recovery and its experimental validation. Sep. Purif. Technol. 190,
582 261-267.
583 Jiang, C., Wang, Q., Li, Y., Wang, Y., Xu, T., 2015. Water electro-transport with
584 hydrated cations in electrodialysis. Desalination 365, 204-212.
585 Kim, J.H., An, B.M., Lim, D.H., Park, J.Y., 2018. Electricity production and
586 phosphorous recovery as struvite from synthetic wastewater using magnesium-air
587 fuel cell electrocoagulation. Water Res. 132, 200-210.

588 Li, R.H., Wang, J.J., Zhang, Z.Q., Awasthi, M.K., Du, D., Dang, P.F., Huan, Q., Zhang,
589 Y.C., Wang, L., 2018. Recovery of phosphate and dissolved organic matter from
590 aqueous solution using a novel CaO-MgO hybrid carbon composite and its
591 feasibility in phosphorus recycling. Sci. Total Environ. 642, 526-536.
592 Li, Y., Shi, S., Cao, H., Wu, X., Zhao, Z., Wang, L., 2016. Bipolar membrane
593 electrodialysis for generation of hydrochloric acid and ammonia from simulated
594 ammonium chloride wastewater. Water Res. 89, 201-209.
595 Lin, T., Gibson, V., Cui, S., Yu, C., Chen, S., Ye, Z., Zhu, Y., 2014. Managing urban
596 nutrient biogeochemistry for sustainable urbanization. Environ. Pollut. 192,
597 244-250.
598 Liu, B., Giannis, A., Zhang, J., Chang, V.W.C., Wang, J., 2013. Characterization of
599 induced struvite formation from source-separated urine using seawater and brine
600 as magnesium sources. Chemosphere 93, 2738-2747.
601 Liu, R., Wang, Y., Wu, G., Luo, J., Wang, S., 2017. Development of a selective
602 electrodialysis for nutrient recovery and desalination during secondary effluent
603 treatment. Chem. Eng. J. 322, 224-233.
604 Lahav, O., Telzhensky, M., Zewuhn, A., Gendel, Y., Gerth, J., Calmano, W., Birnhack,
605 L., 2013. Struvite recovery from municipal-wastewater sludge centrifuge
606 supernatant using seawater NF concentrate as a cheap Mg(II) source. Sep. Purif.
607 Technol. 108, 103-110.
608 Lee, C.G., Alvarez, P.J.J., Kim, H.G., Jeong, S., Lee, S., Lee, K.B., Lee, S.H., Choi,
609 J.W., 2018. Phosphorous recovery from sewage sludge using calcium silicate

610 hydrates. Chemosphere 193, 1087-1093.

611 Marcus, Y., 2012. Ions in water and biophysical implicaitons-From chaos to
612 Cosmos.Springer Dordrecht Heidelberg London NewYork.

613 Masigol, M.A., Moheb, A., Mehrabani-Zeinabad, A., 2012. An experimental
614 investigation into batch electrodialysis process for removal of sodium sulfate from
615 magnesium stearate aqueous slurry. Desalination 300, 12-18.

616 Mehta, C., Tucker, R., Poad, G., Davis, R., McGahan, E., Galloway, J., O'Keefe, M.,
617 Trigger, R., Batstone, D., 2016. Nutrients in Australian agro-industrial residues:
618 production, characteristics and mapping. Australas. J. Environ. Manag. 23 (2),
619 206-222.

620 Mehta, C.M., Khunjar, W.O., Nguyen, V., Tait, S., Batstone, D.J., 2015. Technologies
621 to recover nutrients from waste streams: a critical review. Crit. Rev. Env. Sci.
622 Technol. 45, 385-427.

623 Moerman, W., Carballa, M., Vandekerckhove, A., Derycke, D., Verstraete, W., 2009.
624 Phosphate removal in agro-industry: pilot- and full-scale operational
625 considerations of struvite crystallization. Water Res. 43, 1887 – 1892.

626 National Bureau of Statistics of the People's Republic of China (NBSPRC), 2017. The
627 China Statistical Yearbook 2017. Available online:
628 http://www.stats.gov.cn/tjsj/ndsj/2017/indexch.htm

629 Nie, X., Sun, S., Song, S.Z., Yu, J., 2017. Ion-fractionation of lithium ions from
630 magnesium ions by electrodialysis using monovalent selective ion-exchange
631 membranes. Desalination 403, 128-135.

Nkoa, R., 2014. Agricultural benefits and environmental risks of soil fertilization with anaerobic digestates: a review. Agron. Sustain. Dev. 34, 473-492.

Reig, M., Casas, S., Aladjem, C., Valderrama, C., Gibert, O., Valero, F., Centeno, C.M., Larrotcha, E., Cortina J.L., 2014. Concentration of NaCl from seawater reverse osmosis brines for the chlor-alkali industry by electrodialysis. Desalination, 342, 107-117.

Rottiers, T., De la Marche, G., Van der Bruggen, B., Pinoy, L., 2015. Co-ion fluxes of simple inorganic ions in electrodialysis metathesis and conventional electrodialysis. J. Membr. Sci. 492, 263-270.

Selvaraj, H., Aravind, P., Sundaram, M., Four compartment mono selective electrodialysis for separation of sodium formate from industry wastewater. Chem. Eng. J. 333, 162-169.

Shen, Y., Ye, Z., Ye, X., Wu, J., Chen, S., 2016. Phosphorus recovery from swine wastewater by struvite precipitation: composition and heavy metals in the precipitates. Desalin. Water Treat. 57, 10361-10369.

Shi, L., Hu, Y., Xie, S., Wu, G., Hu, Z., Zhan, X., 2018. Recovery of nutrients and volatile fatty acids from pig manure hydrolysate using two-stage bipolar membrane electrodialysis. Chem. Eng. J. 334, 134-142.

Tado, K., Sakai, F., Sano, Y., Nakayama, A., 2016. An analysis on ion transport process in electrodialysis desalination. Desalination 378, 60-66.

Tadimeti, J.G.D, Chattopadhyay, S., 2016. Physico-chemical local equilibrium influencing cation transport in electrodialysis of multi-ionic solutions.

654 Desalination 385, 93-105.

655 Taddeo, R., Kolppo, K., Lepistö, R., 2016. Sustainable nutrients recovery and
656 recycling by optimizing the chemical addition sequence for struvite precipitation
657 from raw swine slurries. J. Environ. Manage. 180, 52-58.

658 Tedesco, M., Hamelers, H.V.M., Biesheuvel, P.M., 2016. Nernst-Planck transport
659 theory for (reverse) electrodialysis: I. Effect of co-ion transport through the
660 membranes. J. Membr. Sci. 510, 370-381.

661 Tran, A.T.K., Zhang, Y., Lin, J., Mondal, P., Ye, W., Meesschaert, B., Pinoy, L., Van
662 der Bruggen, Bart., 2015. Phosphate pre-concentration from municipal wastewater
663 by selectrodialysis: Effect of competing components. Sep. Purif. Technol. 141,
664 38-47.

665 Wang, X., Zhang, X., Wang, Y., Du, Y., Feng, H., Xu, T., 2015. Simultaneous recovery
666 of ammonium and phosphorus via the integration of electrodialysis with struvite
667 reactor. J. Membr. Sci. 490, 65-71.

668 Ward, A.J., Arola, K., Brewster, E.T., Mehta, C.M., Batstone, D.J., 2018. Nutrient
669 recovery from wastewater through pilot scale electrodialysis. Water Res. 135,
670 57-65.

671 Xie, M., Shon, H.K., Gray, S.R., Elimelech, M., 2016. Membrane-based processes for
672 wastewater nutrient recovery: technology, challengers, and future direction. Water Res.
673 89, 210-221.

674 Ye, Z., Ghyselbrecht, K., Monballiu, A., Rottiers, T., Sansen, B., Pinoy, L.,
675 Meesschaert B., 2018. Fractionating magnesium ion from seawater for struvite

676 recovery using electrodialysis with monovalent selective membranes.
677 Chemosphere, 210, 867-876. 10.1016/j.chemosphere.2018.07.078.
678 Ye, Z., Chen, S., Lu, M., Shi, J., Lin, L., Wang, S., 2011. Recovering phosphorus as
679 struvite from the digested swine wastewater with bittern as a magnesium source.
680 Water Scie. Technol. 64, 334-340.
681 Ye, Z., Deng, Y., Ye, X., Lou, Y., Chen, S., 2018. Application of image processing on
682 struvite recovery from swine wastewater by using the fluidized bed. Water Sci.
683 Technol. 77, 159-166.
684 Ye, Z., Ghyselbrecht, K., Monballiu, A., Rottiers, T., Sansen, B., Pinoy, L.,
685 Meesschaert, B., 2018. Fractionating magnesium ion from seawater for struvite
686 recovery using electrodialysis with monovalent selective membranes.
687 Chemosphere 210, 867-876.
688 Zhang, W., Miao, M., Pan, J., Sotto, A., Shen, J., Gao, C., Van der Bruggen, B., 2017.
689 Separation of divalent ions from seawater concentrate to enhance the purity of
690 coarse salt by electrodialysis with monovalent-selective membranes. Desalination
691 411, 28-37.
692 Zhang, Y., Desmidt, E., Van Looveren, A., Pinoy, L., Messchaert, B., Van der Bruggen,
693 B., 2013. Phosphate separation and recovery from wastewater by novel
694 electrodialysis. Environ. Sci. Technol. 47, 5888-5895.
695 Zhou, K., Barjenbruch, M., Kabbe, C., Inial, G., Remy, C., 2017. Phosphorus
696 recovery from municipal and fertilizer wastewater: China's potential and
697 perspective. J. Environ. Sci. 52, 151-159.

Tables

Table 1 Initial feed, anionic product, cationic product, brine and electrode solutions used in the experiments.

Item	Content	Concentration	Volume
Feed	$NaH_2PO_4 \cdot H_2O$	40 mg-P/L	2 L
	NH_4Cl	500 mg-N/L	
	Na_2SO_4	100 mg-SO_4/L	
	KCl	400 mg-K/L	
	$MgCl_2$	60 mg-Mg/L	
	$CaCl_2$	100 mg-Ca/L	
	NaCl	3.192 mmol/L	
Anionic product	NaCl	0.1 mol/L	1 L
Cationic product	NaCl	0.1 mol/L	1 L
Brine	NaCl	0.1 mol/L	1 L
Electrode solution	Sodium sulfamate	0.1 mol/L	2 L

705

706

707

708

709 **Table 2** Types of membranes and their properties.

Membrane type*	PC-SA	PC-SK	PC-MVK	PC-MVA	PC-SC
Thickness (μm)	200	130	100	110	130
Resistance (Ω cm^2)	~1.8	~2.5	-	~20	~9
Burst strength ($kg \cdot cm^2$)	4-5	4	3	2	15
Transference number (KCl)	>95%	>95%	>97%	>97%	>94%
Temperature (°C)	0-60	0-50	0-40	0-40	0-40
Spacer type	Thickness 0.45 mm, made by silicone/polypropylene, mesh type 45°				

710 *The data were provided by the manufacturer.

711

712

713

714

715

716 **Table 3** Fractionation ratio, energy consumption and current efficiency under different

717 operational modes.

	Item	Constant current	Constant voltage
Fractionation ratio (%)	Mg^{2+}	57.3%	59.6%
	Ca^{2+}	64.0%	63.6%
	NH_4^+	56.2%	63.2%
	K^+	32.9%	37.7%
	PO_4^{3-}	87.1%	89.6%
	SO_4^{2-}	75.9%	76.8%
Energy efficiency	kWh/kg Mg	5.967	6.103
	kWh/kg Ca	6.067	6.638
	kWh/kg PO_4	33.717	28.380
	kWh/kg SO_4	20.019	17.995
	kWh/kg NH_4	0.949	0.783
	kWh/kg K	6.033	5.220
Current efficiency	Mg^{2+}	3.81%	3.67%
	Ca^{2+}	4.54%	4.10%
	NH_4^+	25.27%	30.23%
	K^+	9.64%	11.00%
	PO_4^{3-} -P	2.54%	4.16%
	SO_4^{2-}	2.01%	2.21%

718

719

720

721

722 **Table 4** Properties of ions in the aqueous solution.

Ion	*r* (nm)[a]	*R* (nm)[b]	Hydration free energy (kJ/mol)	Reference
SO_4^{2-}	0.230	0.275	-1113	Marcus, 2012
Cl^-	0.181	0.225	-337	Marcus, 2012
PO_4^{3-}	0.238	0.295	-2379	Marcus, 2012
NH_4^+	0.148	0.331	-29.5	Jiang et al., 2015
K^+	0.149	0.331	-295	Chen et al., 2018
Ca^{2+}	0.100	0.412	-1504	Chen et al., 2018
Mg^{2+}	0.072	0.428	-1828	Chen et al., 2018
Na^+	0.117	0.358	-365	Wang et al., 2015

723 [a]*r*, ionic radii; [b]*R*, hydrated ionic radii.

724

725

726

727

728

729 **Table 5** Energy consumption and current efficiency under different voltages.

	Item	6V	7V	8V	9V	10V
Energy efficiency	kWh/kg $MgCl_2$	17.794	20.098	23.052	24.371	24.659
	kWh/kg $CaCl_2$	14.731	16.080	15.478	17.638	19.214
	kWh/kg NaH_2PO_4	19.741	19.784	24.027	29.554	35.124
	kWh/kg Na_2SO_4	30.777	25.917	25.672	35.063	36.587
	kWh/kg NH_4Cl	1.736	2.629	3.873	3.383	4.425
	kWh/kg KCl	6.663	10.797	16.208	13.247	18.237
Current efficiency	Mg^{2+}	3.80%	3.92%	3.91%	4.16%	1.30%
	Ca^{2+}	3.94%	4.21%	4.99%	4.93%	2.26%
	NH_4^+	31.15%	23.99%	18.61%	23.97%	20.36%
	K^+	12.64%	9.10%	6.93%	9.53%	7.69%
	PO_4^{3-}	4.07%	4.74%	4.46%	4.08%	0.35%
	SO_4^{2-}	1.47%	2.04%	2.35%	1.94%	1.33%

730

731

732

733

734

735 **Table 6** Energy consumption, current efficiency and extraction ratio under different

736 initial phosphate concentrations.

Item	P60	P180	P270	P470
Current efficiency	3.55%	4.05%	2.81%	0.65%
Energy efficiency (kWh/kg NaH_2PO_4)	29.420	25.810	37.243	160.132
Extraction ratio (%)	85.0%	82.1%	60.9%	13.7%

737

738

739

740

741 **Table 7** Elemental analyses on the recovered solids.

Voltage	PO_4-P*		Mg		Ca		SO_4^{2-}	P:Mg:Ca	Calcium phosphate	Magnesium phosphate
	Avr.	sd.	Avr.	sd.	Avr.	sd.	Avr.	molar ratio	(%)	(%)
6 V	0.76	0.04	0.30	0.08	0.93	0.11	ND.	1:0.40:1.23	75.3%	24.7%
8 V	0.80	0.02	0.20	0.13	1.11	0.10	ND.	1:0.25:1.38	85.7%	14.3%
10 V	1.07	0.00	0.34	0.12	1.36	0.11	ND.	1:0.32:1.28	80.4%	19.6%

742 * unit of concentration, mmol/g; Avr., average; sd., standard deviation; ND.,

743 undetected.

744

745

746

Highlight

- Various nutrient anions and cations were fractionated simultaneously for recovery
- Electrodialysis was used by integrating selective anion and cation membranes
- The recovered streams were further paired together to produce high-value products
- Different ions displayed significantly different permeation capabilities
- Phosphate recovery was achieved by using inherent Ca and Mg ions in the wastewater

Declaration of interests

☒ The authors declare that they have no known competing financial interests or personal relationships that could have appeared to influence the work reported in this paper.

☐The authors declare the following financial interests/personal relationships which may be considered as potential competing interests: